Microelectronics Reliability 177 (2026) 116010

Contents lists available at ScienceDirect

Microelectronics Reliability

journal homepage: www.elsevier.com/locate/microrel

Research paper

Neutron irradiation assessment of an Inertial Measurement Unit

V. Pietrosanti [a], T. Minniti [b,*], M. Buffardo [c], S. Francola [c], C. Cazzaniga [d], C.D. Frost [d], M. Kastriotou [d], P. Peliti [e], F. Berton [e], U. Zuccari [e], G. Romanelli [b], R. Senesi [b,f], T.F. Catalano [c], C. Andreani [b,g], G. Campolo [c]

[a] Department of Chemical Science and Technologies, University of Rome "Tor Vergata", Via della Ricerca Scientifica, 1, Rome, 00133, Italy
[b] Department of Physics and NAST Centre, University of Rome "Tor Vergata", Via della Ricerca Scientifica, 1, Rome, 00133, Italy
[c] Thales Alenia Space Italia, Via Saccomuro, 24, Rome, 00131, Italy
[d] ISIS Facility, STFC, Rutherford Appleton Laboratory, Harwell, OX11 0QX, United Kingdom of Great Britain and Northern Ireland
[e] Northrop Grumman Italia, Via Pontina, km 27800, Pomezia, 00071, Italy
[f] Istituto di Struttura della Materia (ISM), Consiglio Nazionale delle Ricerche, Via del Fosso del Cavaliere, 100, Rome, 00133, Italy
[g] IPCB-CNR, Viale F. Kennedy, 54, Naples, 80125, Italy

ARTICLE INFO

Keywords:
Single event effects
Soft errors
Neutrons
Inertial Measurement Unit
Radiation test
Single event functional interrupt

ABSTRACT

The experiment presented in this paper involves the irradiation of an enhanced Inertial Measurement Unit developed by Northrop Grumman Italia and designed for avionics and space applications. The employment of this device at avionic altitudes prompted a necessary evaluation of its suitability and operation in a radiation environment characterized by atmospheric neutrons, particles that can lead to malfunctioning in microelectronics operation through single event effects. The results indicate that atmospheric neutron exposure does not significantly impact the long-term performance of the device, whose functionality remains recoverable. Reliability metrics such as cross-sections and failure in time are derived to assess error frequency and support mitigation strategies for avionics and space applications. The results indicate that velocity measurements are the most susceptible parameter, with a FIT of 209, whereas rotation angles and accelerations are more resilient, exhibiting FIT values of 182 and 173, respectively.

1. Introduction

Radiation in the Earth's atmosphere primarily originates from high-energy cosmic rays, which interact with atmospheric nuclei to produce extensive air showers composed of secondary particles [1,2]. Among these secondaries, neutrons play a dominant role. Their production depends strongly on altitude and latitude due to variations in atmospheric density and geomagnetic shielding. At sea level (New York City), the neutron flux ranges from 13 cm^{-2} h^{-1} [3] to 20 cm^{-2} h^{-1} [4], approximately 300 times lower than that observed at an altitude of 12 km. Measurements of neutron spectra at high-elevation sites report a total fluence rate of (0.113 ± 0.013) cm^{-2} s^{-1} [5]. Because neutrons are uncharged and unaffected by magnetic fields, they can penetrate deeply into aircraft and spacecraft structures, increasing radiation exposure risk [6]. Atmospheric neutrons constitute the primary source of radiation-induced failures in avionics, space, and even terrestrial microelectronics, posing a significant threat to device reliability [7]. These failures typically result from substantial charge deposition, most often initiated by neutron-induced spallation reactions occurring near semiconductor substrates [8,9]. Consequently, atmospheric neutrons are a leading cause of Single Event Effects (SEEs) in avionics and space systems [10,11]. SEEs can be classified as hard, such as Single Event Burnout (SEB), or soft, including Single Event Upset (SEU), Single Event Transient (SET), and Single Event Functional Interrupt (SEFI), the latter generally being recoverable [12,13]. The well-established correlation between SEU rates and neutron flux further demonstrates the dominant role of neutrons in aircraft-related SEE phenomena [14–17].

In this context, the functional verification beyond component-level testing has emerged as a cost-effective strategy for space systems with higher risk tolerance, such as CubeSats. System-level radiation testing can improve confidence in mission success while remaining compatible with schedule and budget constraints. Such testing enables assessment of functional reliability and availability, identification of design and component-level vulnerabilities, evaluation of self-recovery behavior, and validation of mitigation strategies such as derating, transient filtering, and error-correction codes. The primary observable effect at system level is loss of functionality, either temporary or permanent, with criticality classifications described in [18]. As embedded systems continue to grow in density and complexity, robustness cannot rely

* Corresponding author.
E-mail address: triestino.minniti@uniroma2.it (T. Minniti).

https://doi.org/10.1016/j.microrel.2026.116010
Received 26 February 2025; Received in revised form 27 November 2025; Accepted 13 January 2026
Available online 15 January 2026

solely on design and theoretical analysis. Fault injection methods are therefore employed to emulate the effects of cosmic radiation, physical attacks, or hardware trojans, typically modeled as SEUs or Multiple Bit Upsets (MBUs) manifested through bit-flips, bit-sets, or bit-resets [19].

Micro-Electro-Mechanical System (MEMS) technology is particularly well-suited for aerospace and upper-atmosphere use due to its compactness, low mass, and cost-effective fabrication. In this study, an Inertial Navigation System (INS) integrating a Commercial Off-The-Shelf (COTS) MEMS-based Inertial Measurement Unit (IMU) was exposed to an accelerated neutron field replicating the spectral characteristics of atmospheric radiation. The IMU, serving as the core sensing element of the INS, was originally developed for terrestrial and avionic applications. There is limited literature available on neutron irradiation testing of IMUs. Experiments involving both 14 MeV and thermal neutrons [20] have reported disruptions in attitude estimation within INSs, inducing SEFIs that temporarily affect orientation assessment and may compromise data integrity, though without causing permanent device damage. In [21], exposure to pulsed neutron fluences up to 8.7×10^{15} cm^{-2} was shown to degrade MEMS sensor performance, leading to accelerometer failure. Similarly, fast neutron testing in [22] revealed that MEMS operation can be affected through secondary effects such as radiation-induced charge trapping in dielectric materials. Conversely, [23] reported that neutron-induced SEEs did not significantly impact the reliability of certain devices, as leakage currents returned to nominal levels post-irradiation, indicating only soft error occurrences.

Within this context, the present work provides the first experimental evaluation of an IMU operating under accelerated atmospheric-like neutron exposure. The findings underscore the importance of further investigations aimed at characterizing IMU behavior and reliability under high-energy neutron fluxes representative of avionic and space environments.

2. Device under test and irradiation methods

2.1. The eIMU device

The device subjected to accelerated neutron testing is an enhanced Inertial Measurement Unit (eIMU) fabricated on a COTS MEMS-based IMU. It was developed by Northrop Grumman Italia (NGI) for terrestrial and avionics applications. MEMS can be manufactured from a wide range of materials (such as silicon, polymers, metals, ceramics) and operate according to different physical principles (piezoelectric, electrostatic, thermal, electromagnetic) for sensing and actuation. At its core, the eIMU integrates sensors that track rotational and translational movements, such as gyroscopes and accelerometers [24]. This system provides measurements of angular increments ($\Delta\theta$) and velocity increments (Δv) in a fixed coordinate system with respect to its chassis. Gyro and accelerometer temperatures are also provided for accurate thermal modeling, and a Built In Test (BIT) function is implemented to detect eIMU failures during its operation. All relevant data, including inertial measurements, temperature readings, and BIT results, are transmitted to an external navigation processor via standard communication protocols, such as RS-422 or serial digital interface. In addition to the standard inertial outputs, like angular rates and accelerations, the eIMU is embedded with GPS-aided navigation sensors, like magnetometer, inclinometer, and barometer, enabling the determination of navigation coordinates through satellite triangulation. Thanks to its small size, low weight and power consumption, the eIMU is well-suited for a variety of applications, including: unmanned systems, platform and gimbal stabilization, attitude and heading reference systems, GPS-aided navigation with altimeter, factory and industrial automation and leveling instruments. Fig. 1 shows a high-level schematic block diagram of the eIMU, outlining its internal structure and the main functional blocks.

The IMU under test in this work does not incorporate radiation-hardened components specifically designed for space or terrestrial radiation environments. Therefore, the effect of neutron exposure was evaluated through accelerated testing of the complete device, ensuring that all components were subjected to the irradiation field, without isolating internal subsystems or employing observables tailored to monitor radiation effects on individual components. This justified a phenomenological approach focused on identifying failure modes at the device level, rather than assessing the intrinsic radiation tolerance of specific electronic elements. It is worth noting that design-level radiation hardening was not considered, as such modifications are not applicable to COTS-based systems.

2.2. Neutron irradiation experiment

The irradiation experiment was conducted at the ChipIr beamline of the ISIS Neutron and Muon Source (Rutherford Appleton Laboratory, UK), which provides a fast, atmospheric-like neutron spectrum tailored for studying SEEs in microelectronics. With a flux of approximately 5×10^6 cm^{-2} s^{-1} between 10 and 800 MeV and a beam size of 70×70 mm^2, ChipIr enables accelerated testing equivalent to over hundreds of years of atmospheric exposure in just one hour. Beam uniformity of ChipIr has been characterized in [25], for further information regarding the beamline configuration and characteristics, see Refs. [25,26].

The experiment was performed by connecting the eIMU to a power supply via its interface (see Fig. 2a). All system components were interfaced with dedicated Electrical Ground Support Equipment (EGSE), which included custom software, developed by NGI, for real-time data acquisition and storage. The power supply voltage provided through the upstream harness was configured at the beginning of the test and maintained at a stable level throughout the irradiation campaign. The irradiation was performed along all three orthogonal axes of the device (see Figs. 2b, c, d) at two distinct positions from the source, namely 14.4 m and 18.2 m. The uncertainty in the measured distance from the source is approximately 4%, corresponding to values of (14.4 ± 0.58) m and (18.2 ± 0.73) m. These distances correspond to different levels of neutron flux, due to the beam's attenuation with increasing distance from the source.

It has been demonstrated that the ChipIr neutron beam is uniform inside an area of 70×70 mm^2 and this dimension provides a typical configuration for electronic device irradiation [25]. For this reason, the size of the neutron beam chosen for the entire duration of the experiment was 70×70 mm^2, which assured a uniform map of the neutron flux on the device. The irradiated area was slightly larger than the eIMU size (66 mm × 56 mm × 28 mm), so that the device could be irradiated evenly everywhere. A laser was used for the alignment of the device at the center of the neutron beam.

During the irradiation tests, the eIMU gyroscope recorded the rotation angles (heading, pitch, roll) and angular velocities (along X, Y, Z axes); the accelerometers recorded the accelerations (along X, Y, Z axes) and velocities (north, east, vertical).

3. Results and discussion

The neutron fluence was determined considering the average neutron count rate, the irradiation time, a conversion factor, and an attenuation factor. The conversion factor reflects the calibrated counting efficiency of the neutron detector and is established at the beginning of each ISIS beam cycle. The attenuation factor accounts for the reduction in neutron fluence with distance and is defined according to the inverse square law relative to the effective distance from the idealized point-like neutron source (located 13.9 m upstream of the ChipIr blockhouse), as detailed in [27]. The resulting neutron fluence values represent the integrated fluence measured up to the point at which a failure is observed. The total cumulative fluence experienced by the eIMU throughout the experimental campaign is reported herein. During the tests, the eIMU was positioned at two distinct distances from the neutron source, specifically at 14.4 m and 18.2 m, which correspond

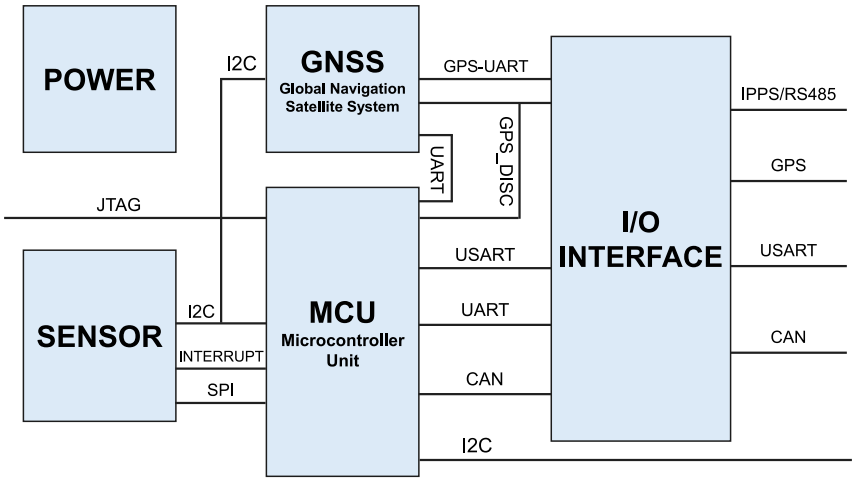

Fig. 1. Schematic block diagram of the eIMU, with the device internal structure and main functional blocks.

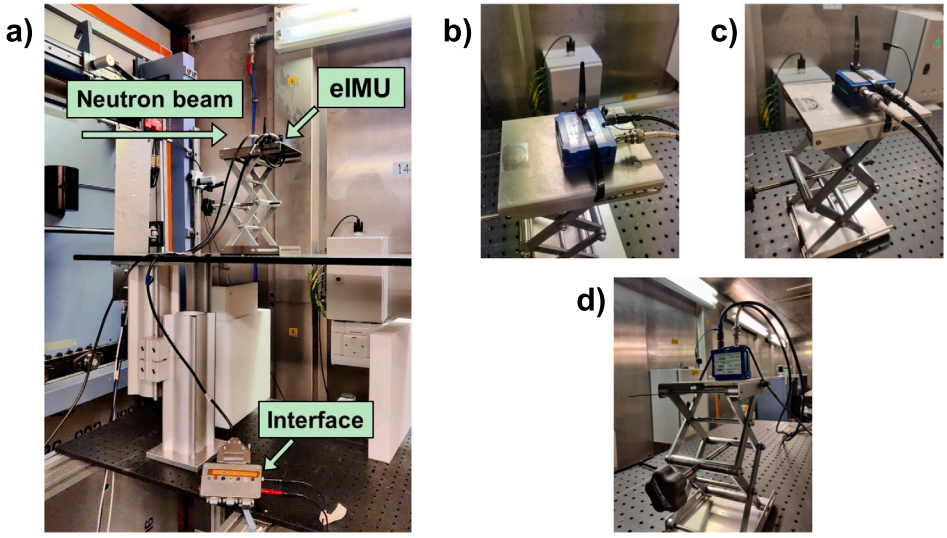

Fig. 2. (a) Experimental setup implemented, showing the ChipIr neutron beam direction and the connection of the eIMU to the interface that links the control software. Pictures showing the three positions of the eIMU, corresponding to the three (b) X, (c) Y and (d) Z axes, chosen for the irradiation tests.

to attenuation factors of the neutron beam of, respectively, 93% and 58%.

The supply current is a direct observable monitored during the irradiation test to assess whether neutron exposure induced overconsumption that could potentially result in destructive failure. The current drawn by the device during operation was measured upstream, directly at the output of the power supply. This monitoring aimed to evaluate whether the current reached critical levels under neutron flux conditions, which would necessitate the implementation of over-current protection mechanisms. The current consumption of the device was not constant over time but exhibited temporal fluctuations. Fig. 3 shows the time evolution of the supply current, highlighting its temporal fluctuations. Once the initial offset required for the device to reach steady-state operation is removed, the current oscillates around an average value of approximately 465 mA and reaches a maximum of 580 mA.

Disruptions caused by neutron interactions manifested as observable deviations in the recorded parameters (angles, accelerations, and velocities). The device specification defines nominal operating ranges for these parameters, beyond which functionality is considered degraded. These ranges are summarized in Table 1.

Fig. 4 presents the behavior of the monitored parameters under non-irradiated conditions. In the static regime, all parameter values remain

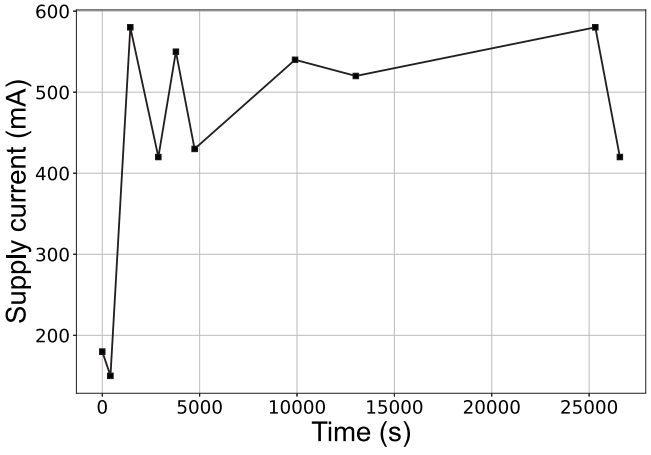

Fig. 3. Time evolution of the supply current, showing the transient behavior and subsequent oscillations around an average value of approximately 465 mA after the device reaches its steady-state operation.

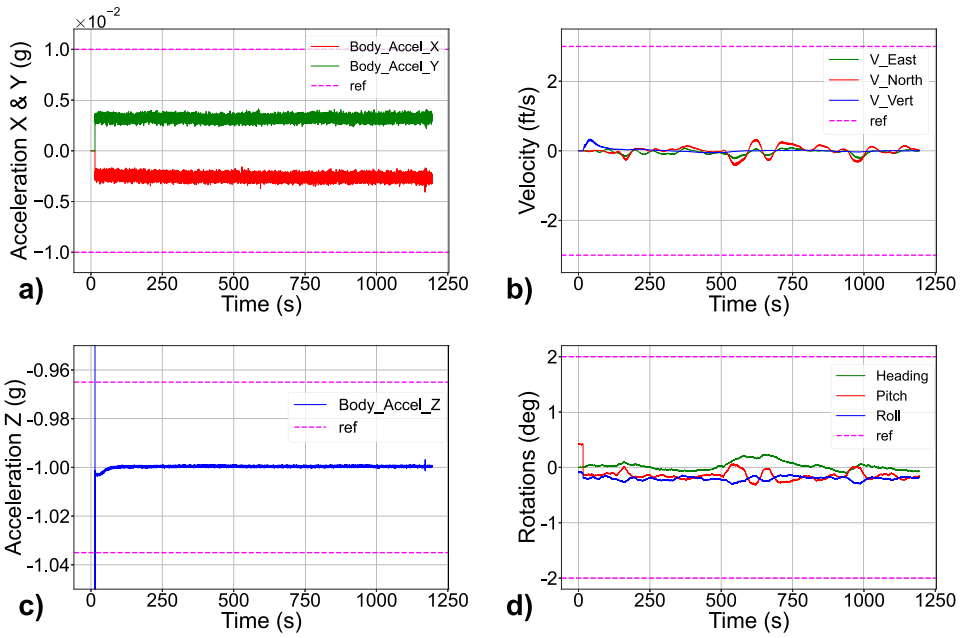

Fig. 4. Plots showing the trends of parameters in the absence of irradiation: (a) accelerations along X and Y axes, (b) velocities, (c) acceleration along Z and (d) rotations. All measurements have been performed along each of the three orthogonal axes of the eIMU.

Table 1
Functioning intervals of the parameters, with nominal, minimum, and maximum values.

Parameters	Nominal	Minimum	Maximum
Rotation angles	0 deg	−1 deg	1 deg
Velocities	0 ft/s	−3 ft/s	3 ft/s
Acceleration X	−0.26 g	−0.25 g	−0.27 g
Acceleration Y	0 g	−0.01 g	0.01 g
Acceleration Z	−0.97 g	−0.96 g	−0.98 g

within their nominal specification range, indicated by the red dashed lines. This baseline enables the identification of out-of-range events and supports the attribution of the observed oscillations to noise, as similar fluctuations were also detected during neutron irradiation.

In most cases, the device was able to correct errors via an internal software and resumed the acquisition, but in many cases, it stopped recording, and a manual restart of the power supply was necessary. The number and types of resets that occurred during the experiment were monitored and divided into manual and automatic types. A manual reset occurred when the device interrupted its operation without restarting, so that an external manual restart was executed by power cycling. An automatic reset was performed by the device's internal code, which automatically resumed the acquisition when the device stopped its operation. The analysis of the type and frequency of resets provides an estimate of the expected need for external intervention in the final application.

The core of the analysis involved classifying the observed events based on the type of SEE induced by neutron interactions within the device. A comparable classification approach is also presented in [28]. The categorization of events was established considering two major SEE phenomena [12] that occurred inside the device when irradiated: SEFI and SET. SEFI is triggered when the values of parameters go out-of-range beyond the permitted time window until a manual reset is performed to bring the parameter back into specifications. SET is triggered when the values of parameters go out-of-range for a short time, corresponding to the maximum permitted limit, automatically going back into specifications. Based on this, the observed events were categorized according to the following considerations:

- step (SEFI): the parameter goes out-of-range and stays there. The trend assumes a step shape;
- drift (SEFI): the parameter goes out-of-range at a certain point of the acquisition, without returning into specifications;
- oscillations (SEFI): a single SEFI occurs, but in the form of continuous oscillations going out-of-range;
- spikes (SET): single event that goes out of specification for a short time, eventually returning inside it. Spikes only cause a temporary malfunction of the device, which is able to perform a correction, returning to its nominal operation.

Fig. 5 shows examples of how categorized events (SEFI, SET) appear in the parameter plots. The categorization of events was based on this observability. Data were retrieved from log files recorded during the experiment, and proper scripts were developed to read and extract data of interest. The experimental procedure was employed to record the number of failures registered by the device, defined as cases in which parameter values exceeded their nominal ranges. Table 1 illustrates the predefined ranges used as input in the scripts for each parameter. This information shows that the interaction of neutrons with the device produced errors that were reflected in the incorrect detection of parameters, whose usual operation was altered. Each observable was treated independently in the SEFI analysis to adopt a conservative, worst-case approach in terms of cross-section values. This was justified by the physical separation of the eIMU sensing elements, the absence of observable correlations in the data, and the unit-level testing, which prevented attributing SEFIs to specific internal components.

Fig. 6 illustrates the trend between the total number of SEFI events and the cumulative neutron fluence for each observable. The error bars on the x-axis were determined based on the average uncertainty of the ChipIr neutron flux, which is approximately 14%, while the y-axis error bars were calculated using Poisson statistics ($\sqrt{N}$). As expected, the data confirms a clear increasing trend, reflecting the accumulation of SEFI events with increasing neutron exposure over successive runs.

Table 2 reports the monitored parameters, including the Failure in Time (FIT) rate, where 1 FIT corresponds to one failure per 10^9 h of device operation. FIT values are derived from the Mean Time To Failure (MTTF), defined as the average operating time between successive failure events. For the MTTF estimation, a reference neutron flux at

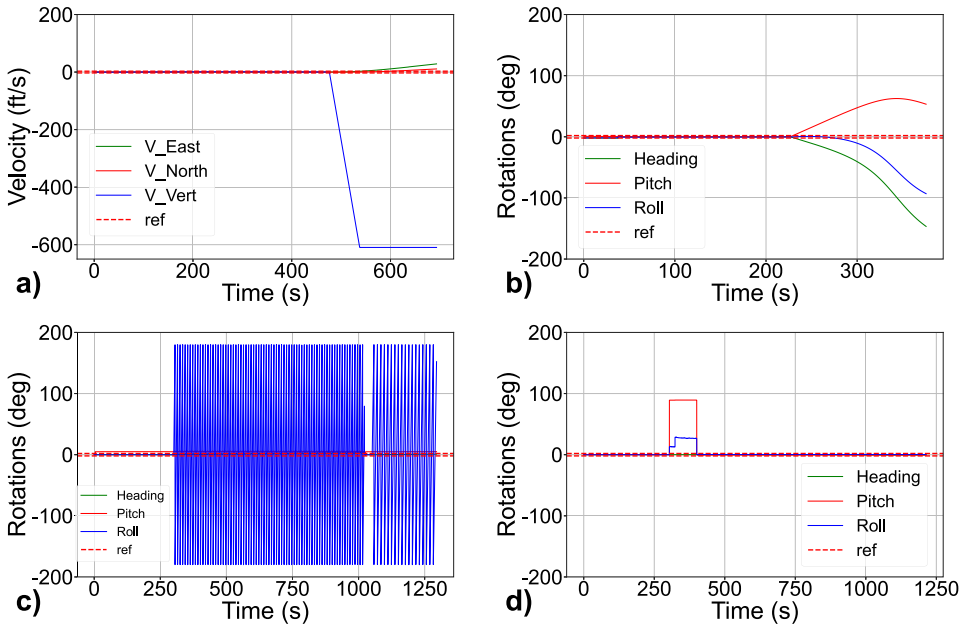

Fig. 5. Examples showing how the categorized errors (SEFI, SET) appear in the parameter plots (the red dashed lines refer to the specification range of each parameter). (a) SEFI assuming a step shape. (b) SEFI drift. (c) Oscillations going out of the reference range. (d) Example of a spike. The eIMU was oriented along its (a) Y, (b) Y, (c) Z, and (d) Z axes during the respective measurements.

Table 2
Data about the total number of events, total neutron fluences, cross-sections and MTTF relative to the three main observables.

Obs.	Tot.no. SEFI	Neutron fluence (cm^{-2})	Cross-section (cm^2)	Failure in time (FIT)
Rot.	10	$(2.15 \pm 0.30) \cdot 10^{11}$	$(4.65 \pm 1.61) \cdot 10^{-11}$	87 < 182 < 334
Accel.	10	$(2.25 \pm 0.32) \cdot 10^{11}$	$(4.44 \pm 1.53) \cdot 10^{-11}$	83 < 173 < 318
Vel.	12	$(2.24 \pm 0.31) \cdot 10^{11}$	$(5.36 \pm 1.72) \cdot 10^{-11}$	108 < 209 < 365

Table 3
SEFI events recovered by an automatic restart (sub-categorization of SEFI). There is information about the number of automatic SEFI, cross-sections and MTTF according to each observable.

Observable	No. automatic SEFI	Automatic cross-section (cm^2)	Automatic failure in time (FIT)
Rotation	3	$(1.40 \pm 0.83) \cdot 10^{-11}$	11 < 55 < 159
Acceleration	2	$(8.88 \pm 6.40) \cdot 10^{-12}$	4 < 35 < 125
Velocity	4	$(1.79 \pm 0.93) \cdot 10^{-11}$	19 < 70 < 178

Table 4
SEFI events recovered by a Power On Reset (POR) restart (sub-categorization of SEFI). There is information about the number of POR SEFI, cross-sections and MTTF according to each observable.

Observable	No. POR SEFI	POR cross-section (cm^2)	POR Failure in time (FIT)
Rotation	7	$(3.26 \pm 1.31) \cdot 10^{-11}$	51 < 127 < 262
Acceleration	8	$(3.55 \pm 1.35) \cdot 10^{-11}$	60 < 139 < 273
Velocity	8	$(3.58 \pm 1.36) \cdot 10^{-11}$	60 < 140 < 275

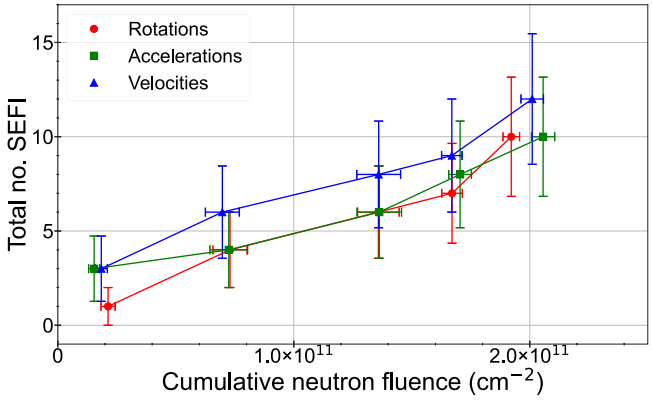

Fig. 6. Trend of the total number of SEFI events and the cumulative neutron fluence, along with the respective uncertainties. This trend highlights a monotonic increase in SEFI occurrences with increasing neutron exposure.

flight altitudes was assumed to be approximately 300 times higher than the ground-level flux measured in New York City, corresponding to 13 cm^{-2} h^{-1} and increasing with altitude [3]. The MTTF was computed based on the expected exposure time to experimental-equivalent fluxes at flight altitudes and on the number of recorded SEFIs. Confidence intervals for the FIT values were calculated according to JEDEC standard JEP151 [29]. These metrics provide valuable insight into the suitability of the device for avionic applications, relative to specific program requirements. The calculated FIT values indicate that velocity measurements are the least resilient parameter, with 209 FIT and an associated MTTF of 4.78 × 10^6 h. By contrast, rotation angles and accelerations exhibit lower FIT values of 182 and 173, corresponding to MTTFs of 5.51 × 10^6 h and 5.78 × 10^6 h, respectively.

From an operative point of view, a sub-categorization of the presented data could be identified for each observables, according to the type of recovery when a SEFI occurred. SEFI errors could be recovered either via an automatic reset, performed by the device, or via a manual reset, performed externally by the user with power cycle. This distinction shows in more detail the type of SEFI events that occurred and how

Table 5
Number of SEFIs recorded for each observable and the total count, reported for two distinct eIMU distances from the beam entrance, together with the corresponding cumulative integrated fluence.

Distance (m)	Neutron fluence (cm^{-2})	SEFI rotation	SEFI acceleration	SEFI velocity	SEFI tot
14.4	1.64×10^{11}	7	9	8	24
18.2	5.82×10^{10}	3	1	4	8

Table 6
Table presenting the SEFI event timestamps, recovery mode, and per-run fluence for each observable and at the two tested distances. Timestamps are referenced to the start time of each acquisition file within a run. The recovery modes are indicated as M (manual) and A (automatic).

Observable	Distance (m)	Timestamp (s)	Recovery mode	Per-run fluence (cm^{-2})
Rotations	14.4	225	M	1.36E+09
	18.2	300	A	1.13E+09
		2750	M	1.04E+10
		1100	M	4.15E+09
	14.4	45	A	1.78E+08
		1450	M	5.48E+09
	14.4	220	M	8.31E+08
	14.4	480	M	1.81E+09
		750	A	2.83E+09
		1250	M	4.72E+09
Accelerations	14.4	500	A	3.01E+09
		225	M	9.04E+08
		450	A	2.71E+09
	18.2	1000	M	3.78E+09
	14.4	1250	M	7.53E+09
		5404	M	3.26E+10
	14.4	50	M	3.01E+08
		1012	M	6.10E+09
	14.4	480	M	2.89E+09
		1250	M	7.53E+09
Velocities	14.4	950	A	5.72E+09
		200	M	1.20E+09
		450	M	2.71E+09
	18.2	300	A	1.13E+09
		2750	M	1.04E+10
		1000	M	3.78E+09
	14.4	50	A	3.01E+08
		1450	M	8.73E+09
	14.4	100	M	6.02E+08
	14.4	490	M	2.95E+09
		770	A	4.64E+09
		1300	M	7.83E+09

we handled the device interruption. The aim is to provide a strategy for managing malfunctions and failures, and what action to take for a device application. The recovery time was approximately 10 s, and the resulting dead time in all irradiation measurements ranged between 0.5% and 2% of the total test duration. This indicates that the impact of the recovery period can be considered negligible compared to the overall irradiation time.

Tables 3 and 4 show, respectively, the two sub-categorizations of SEFI events according to both automatic and manual (defined as Power On Reset, POR) SEFI recovery, displaying information about the number of SEFI, cross-sections and MTTF. The presented data include all the categorizations of SEFI types described before, i.e., step, drift and oscillations. The SET event is not inserted as it has a short duration and does not require an external intervention. The sub-categorization of SEFI events further reveals a clear trend in parameter resilience. Specifically, rotation angles indicate a higher susceptibility to radiation-induced disruptions, exhibiting automatic MTTFs of 55 FIT and POR MTTF of 163 FIT. In contrast, accelerations and velocities show improved resilience, with automatic MTTFs totaling 84 FIT and 87 FIT, respectively, and POR MTTFs amounting to 234 FIT and 209 FIT. These results further suggest that acceleration and velocity parameters tend to experience lower frequencies of failure or under higher levels of neutron fluence, compared to angular measurements. By adopting a phenomenological approach, the categorization of SEEs can provide insights into the possible origin of the events based on the unit's block diagram.

Table 5 reports the number of SEFIs detected for each observable, along with the total count and the cumulative integrated neutron fluence for the two eIMU distances from the beam entrance. The results indicate that the number of SEFIs is directly dependent on the total neutron fluence accumulated by the device during irradiation. The ratio between the two fluence values is approximately 36%, which implies an expected SEFI number of 8 to 9 events at 18.2 m, consistent with observations. However, the statistical confidence at the 18.2 m position was limited due to a beam loss event during testing, preventing the achievement of a fluence compatible to the one at 14.4 m.

The structure of the unit highlights the presence of both digital components, such as the MCU, and analog-oriented blocks, including the sensor, power supply, and I/O interface. From this perspective, transient SEFIs are more likely to be caused by the propagation of SEEs originating in the sensor block or the I/O interface. These effects are often self-recovering and may result from perturbations in the measurement chain or transients generated by sensor or interface electronics. On the other hand, persistent SEFIs, such as drift, step changes, or oscillations, are typically associated with digital electronics. For example, a bit-flip in memory could cause the MCU to incorrectly integrate sensor signals. In particular, SEFIs that can be recovered by a reset support this interpretation, as a reset operation restores memory states and can thereby clear SEUs responsible for the observed malfunctions.

4. Conclusions

This work presented an irradiation experiment performed with an atmospheric-like accelerated neutron spectrum on a gyroscope (eIMU) designed for aircraft and small satellite control. The analysis focused on identifying and classifying malfunction events according to SEE types, providing an overview of the eIMU behavior through the recorded parameters. The calculated neutron fluences and failure in time values offered quantitative insight into the device response under neutron exposure. The results confirm the probabilistic nature of neutron interactions, as neutrons strike the sensitive volume of the device in a random and non-deterministic manner. Despite exposure to high neutron fluences, no permanent damage was observed; all detected anomalies were transient and recoverable, either through power cycling or by onboard error-correcting mechanisms. Failure in time analysis further indicated that velocity measurements are the most susceptible to neutron-induced disturbances, whereas rotation and acceleration data show higher resilience, with failures occurring less frequently or at later exposure times.

4.1. Future work

It should be emphasized that this study does not aim to qualify the device for space applications. The space radiation environment includes not only atmospheric-like neutrons but also charged

particles such as protons and heavy ions, which can generate secondary neutrons through interactions with spacecraft structures or planetary surfaces [30,31]. For potential space use of the eIMU, further investigations should assess failure modes related to data bus communication and supply current behavior. Issues such as frozen interfaces or incorrect responses require appropriate fault management strategies. While a satellite reset procedure can often restore nominal operation, recurring or persistent faults might necessitate hardware redesigns. The supply current, a critical parameter in spacecraft architecture, showed temporal fluctuations with no evident correlation to SEE occurrences; however, the implementation of upstream overcurrent protection could mitigate potential risks. This study provides an initial characterization of the eIMU response under high atmospheric-like neutron fluxes, offering valuable insight into its radiation tolerance. Nevertheless, comprehensive qualification for specific missions will require tailored evaluations that account for unique operational environments and reliability requirements.

The need for effective mitigation techniques against radiation-induced degradation in high-flux conditions is well recognized in the literature [20,32]. In particular, [20] emphasizes that frequent SEFI events under elevated neutron fluxes or prolonged exposure may demand adapted mitigation strategies. As discussed in [33,34], the design of neutron shielding requires careful material selection and validation through dedicated experimental studies [35]. The application of dedicated shielding for the eIMU thus represents a promising direction for future research. Simulation campaigns will be conducted prior to further neutron testing to identify the most suitable materials and to assess the effects of neutron interactions on device performance.

CRediT authorship contribution statement

V. Pietrosanti: Conceptualization, Methodology, Formal analysis, Investigation, Data curation, Writing – original draft, Visualization. **T. Minniti:** Software, Validation, Resources, Data curation, Validation, Writing – original draft, Writing – review & editing, Supervision, Project administration. **M. Buffardo:** Conceptualization, Investigation, Writing – review & editing. **S. Francola:** Data curation, Validation, Supervision, Writing – original draft, Writing – review editing. **C. Cazzaniga:** Investigation, Writing – review & editing. **C.D. Frost:** Writing – review & editing. **M. Kastriotou:** Investigation, Writing – review & editing. **P. Peliti:** Writing – review & editing. **F. Berton:** Investigation, Writing – review & editing. **U. Zuccari:** Investigation, Writing – review & editing. **G. Romanelli:** Investigation, Writing – review & editing. **R. Senesi:** Writing – review & editing. **T.F. Catalano:** Writing – review & editing. **C. Andreani:** Conceptualization, Writing – review & editing, Funding acquisition. **G. Campolo:** Conceptualization, Writing – review & editing, Funding acquisition.

Declaration of competing interest

The authors declare that they have no known competing financial interests or personal relationships that could have appeared to influence the work reported in this paper.

Acknowledgments

The authors gratefully acknowledge the support of the ISIS@MACH ITALIA Research Infrastructure, the hub of ISIS Neutron and Muon Source (UK), (MUR official registry No. U. 0008642.28-05-2020—April 16, 2020). The financial support from the Consiglio Nazionale delle Ricerche within the CNR-STFC Grant Agreement (No.2021–2027) concerning collaboration in scientific research at the ISIS (UK) of STFC is gratefully acknowledged. The STFC Rutherford Appleton Laboratory is acknowledged for its access to the neutron beam at the ChipIr facility.

Appendix

Table 6 reports detailed information on the detected SEFI events collected for each observable during the irradiation tests. The table includes event timestamps, recovery modes, and the corresponding accumulated fluence values for each run at the two tested distances. Timestamps are referenced to the start time of each acquisition file within a run. Recovery modes are classified as manual (M) or automatic (A), indicating whether user intervention was required or if the system recovered autonomously.

Data availability

Data will be made available on request.

References

[1] P.K. Grieder, Extensive Air Showers: High Energy Phenomena and Astrophysical Aspects-A Tutorial, Reference Manual and Data Book, Springer Science & Business Media, 2010, http://dx.doi.org/10.1007/978-3-540-76941-5.
[2] T.K. Gaisser, R. Engel, E. Resconi, Cosmic rays and particle physics, Cambridge University Press, 2016.
[3] Process Management for Avionics—Atmospheric Radiation Effects. Guidelines for Single Event Effects Testing for Avionics Systems, IEC Standard 62396-2, Tech. rep., International Electrotechnical Commission: Geneva, Switzerland, 2017.
[4] M. Cecchetto, R. García Alía, F. Wrobel, Impact of energy dependence on ground level and avionic SEE rate prediction when applying standard test procedures, Aerospace 6 (11) (2019) http://dx.doi.org/10.3390/aerospace6110119.
[5] R. Bedogni, A. Fontanilla, A. Calamida, A.C. Campoy, L. Russo, V. Monti, E. Mafucci, C. Vigorito, S. Vernetto, A. Pietropaolo, Cosmic neutrons at ground: new spectral measurements at 3480 m asl and benchmarking of the cascade component as a function of the elevation at around 45° geomagnetic latitude, Eur. Phys. J. Plus 138 (5) (2023) 421.
[6] M. Shea, D. Smart, Cosmic ray implications for human health, Space Sci. Rev. 93 (2000) 187–205, http://dx.doi.org/10.1023/A:1026544528473.
[7] L. Desorgher, E. Flückiger, M. Gurtner, M. Moser, R. Bütikofer, Atmocosmics: A geant 4 code for computing the interaction of cosmic rays with the Earth's atmosphere, Internat. J. Modern Phys. A 20 (29) (2005) 6802–6804, http://dx.doi.org/10.1142/S0217751X05030132.
[8] G. Soelkner, Ensuring the reliability of power electronic devices with regard to terrestrial cosmic radiation, Microelectron. Reliab. 58 (2016) 39–50, http://dx.doi.org/10.1016/j.microrel.2015.12.019.
[9] J.F. Ziegler, Terrestrial cosmic rays, IBM J. Res. Dev. 40 (1) (1996) 19–39, http://dx.doi.org/10.1147/rd.401.0019.
[10] E. Petersen, Single Event Effects in Aerospace, John Wiley & Sons, 2011, http://dx.doi.org/10.1002/9781118084328.
[11] R. Velazco, D. McMorrow, J. Estela, Radiation Effects on Integrated Circuits and Systems for Space Applications, Springer, 2019, http://dx.doi.org/10.1007/978-3-030-04660-6.
[12] R. Bolinder, Atmospheric Radiation Effects Study on Avionics: An Analysis of NFF Errors, (Dissertation), 2013, Available at: https://urn.kb.se/resolve?urn=urn:nbn:se:liu:diva-96726.
[13] H. Quinn, The use of accelerated radiation testing for avionics, in: AIP Conference Proceedings, vol. 1525, (1) American Institute of Physics, 2013, pp. 643–648, http://dx.doi.org/10.1063/1.4802406.
[14] M.M. Meier, K. Copeland, K.E. Klöble, D. Matthiä, M.C. Plettenberg, K. Schennetten, M. Wirtz, C.E. Hellweg, Radiation in the atmosphere—A hazard to aviation safety? Atmosphere 11 (12) (2020) 1358, http://dx.doi.org/10.3390/atmos11121358.
[15] A. Taber, E. Normand, Single event upset in avionics, IEEE Trans. Nucl. Sci. 40 (2) (1993) 120–126, http://dx.doi.org/10.1109/23.212327.
[16] E. Normand, Single-event effects in avionics, IEEE Trans. Nucl. Sci. 43 (2) (1996) 461–474, http://dx.doi.org/10.1109/23.490893.
[17] E. Normand, T. Baker, Altitude and latitude variations in avionics SEU and atmospheric neutron flux, IEEE Trans. Nucl. Sci. 40 (6) (1993) 1484–1490, http://dx.doi.org/10.1109/23.273514.
[18] A. Coronetti, R.G. Alía, J. Budroweit, T. Rajkowski, I.D.C. Lopes, K. Niskanen, D. Söderström, C. Cazzaniga, R. Ferraro, S. Danzeca, et al., Radiation hardness assurance through system-level testing: Risk acceptance, facility requirements, test methodology, and data exploitation, IEEE Trans. Nucl. Sci. 68 (5) (2021) 958–969, http://dx.doi.org/10.1109/TNS.2021.3061197.
[19] Z.U. Abideen, M. Rashid, EFIC-ME: a fast emulation based fault injection control and monitoring enhancement, IEEE Access 8 (2020) 207705–207716.

[20] T.K.S. Sartori, H. Fourati, M. Letiche, R.P. Bastos, Assessment of radiation effects on attitude estimation processing for autonomous things, IEEE Trans. Nucl. Sci. 69 (7) (2022) 1610–1617, http://dx.doi.org/10.1109/TNS.2022.3176676.

[21] K. Holbert, S.S. McCready, A.S. Heger, T.H. Harlow, D.R. Spearing, Performance of piezoresistive and piezoelectric sensors in pulsed reactor experiments, in: American Nuclear Society 4th International Topical Meeting on Nuclear Plant Instrumentation, Control and Human Machine Interface Technology, 2004, pp. 43–50, Available at: https://www.scopus.com/record/display.uri?eid=2-s2.0-32044468097&origin=inward&txGid=58d201e4d31069406af7721c0707c151.

[22] P. Gkotsis, V. Kilchytska, C. Fragkiadakis, P.B. Kirby, J.-P. Raskin, L.A. Francis, Effects of fast neutrons on the electromechanical properties of materials used in microsystems, J. Microelectromech. Syst. 21 (6) (2012) 1471–1483, http://dx.doi.org/10.1109/JMEMS.2012.2211578.

[23] S.T. Patton, A.J. Frasca, J.W. Talnagi, D.J. Hyman, B.S. Phillips, J.G. Jones, R.A. Vaia, A.A. Voevodin, Effect of space radiation on the leakage current of MEMS insulators, IEEE Trans. Nucl. Sci. 60 (4) (2013) 3074–3083, http://dx.doi.org/10.1109/TNS.2013.2263840.

[24] T.K.S. Sartori, L.H. Laurini, H. Fourati, R.P. Bastos, Effectiveness of attitude estimation processing approaches in tolerating radiation soft errors, IEEE Trans. Nucl. Sci. 70 (8) (2023) 1658–1665, http://dx.doi.org/10.1109/TNS.2023.3284991.

[25] C. Cazzaniga, C.D. Frost, Progress of the scientific commissioning of a fast neutron beamline for chip irradiation, J. Phys.: Conf. Ser. 1021 (2018) 012037, http://dx.doi.org/10.1088/1742-6596/1021/1/012037, IOP Publishing.

[26] C. Cazzaniga, N. Bhuiyan, M. Kastriotou, D. Chiesa, S. Lilley, C.D. Frost, Fast neutron measurements for the characterization of the ChipIr beamline, IEEE Trans. Nucl. Sci. (2024) http://dx.doi.org/10.1109/TNS.2024.3416540.

[27] C. Cazzaniga, M. Bagatin, S. Gerardin, A. Costantino, C.D. Frost, First tests of a new facility for device-level, board-level and system-level neutron irradiation of microelectronics, IEEE Trans. Emerg. Top. Comput. 9 (1) (2018) 104–108, http://dx.doi.org/10.1109/TETC.2018.2879027.

[28] G. Bazzano, A. Ampollini, F. Cardelli, F. Fortini, P. Nenzi, G. Palmerini, L. Picardi, L. Piersanti, C. Ronsivalle, V. Surrenti, et al., Radiation testing of a commercial 6-axis MEMS inertial navigation unit at ENEA frascati proton linear accelerator, Adv. Space Res. 67 (4) (2021) 1379–1391, http://dx.doi.org/10.1016/j.asr.2020.11.031.

[29] JEDEC Solid State Technology Association, JEP151: Test procedure for the measurement of terrestrial cosmic ray induced destructive effects in power semiconductor devices, 2010, Available: https://www.jedec.org/standards-documents/docs/jep151, JEDEC Publication.

[30] C. Andreani, R. Senesi, A. Paccagnella, M. Bagatin, S. Gerardin, C. Cazzaniga, C. Frost, P. Picozza, G. Gorini, R. Mancini, et al., Fast neutron irradiation tests of flash memories used in space environment at the ISIS spallation neutron source, AIP Adv. 8 (2) (2018) http://dx.doi.org/10.1063/1.5017945.

[31] J. Adams, M. Bhattacharya, Z.-W. Lin, G. Pendleton, J. Watts, The ionizing radiation environment on the moon, Adv. Space Res. 40 (3) (2007) 338–341, http://dx.doi.org/10.1016/j.asr.2007.05.032.

[32] H.R. Shea, Effects of radiation on mems, in: Reliability, Packaging, Testing, and Characterization of MEMS/MOEMS and Nanodevices X, vol. 7928, SPIE, 2011, pp. 96–108, http://dx.doi.org/10.1117/12.876968.

[33] T. Piotrowski, Neutron shielding evaluation of concretes and mortars: A review, Constr. Build. Mater. 277 (2021) 122238, http://dx.doi.org/10.1016/j.conbuildmat.2020.122238.

[34] S.T. Abdulrahman, Z. Ahmad, S. Thomas, A.A. Rahman, Introduction to neutron-shielding materials, in: Micro and Nanostructured Composite Materials for Neutron Shielding Applications, Elsevier, 2020, pp. 1–23, http://dx.doi.org/10.1016/B978-0-12-819459-1.00001-5.

[35] M. Martellucci, G. Romanelli, S. Valeri, D. Cottone, C. Andreani, R. Senesi, The neutron cross section of barite-enriched concrete for radioprotection shielding in the range 1 meV–1 keV, Eur. Phys. J. Plus 136 (2) (2021) 259, http://dx.doi.org/10.1140/epjp/s13360-021-01243-z.